Carbohydrate Polymers 112 (2014) 494–501

Contents lists available at ScienceDirect

Carbohydrate Polymers

journal homepage: www.elsevier.com/locate/carbpol

Gas permeability and selectivity of cellulose nanocrystals films (layers) deposited by spin coating

Martha A. Herrera, Aji P. Mathew, Kristiina Oksman*

Division of Materials Science, Luleå University of Technology, SE-97187 Luleå, Sweden

ARTICLE INFO

Article history:
Received 10 November 2013
Received in revised form 5 June 2014
Accepted 6 June 2014
Available online 20 June 2014

Poly(allylamine hydrochloride) (PubChem CID: 82291)

Keywords:
Cellulose nanocrystal
Surface charge
Spin coating
Gas permeability
Gas selectivity

ABSTRACT

Cellulose nanocrystals (CNC) were extracted from a cellulose residue using two different acid hydrolysis procedures. CNC extracted with sulfuric acid (CNC_S) showed higher surface charge (339 μmol/g) compared with crystals extracted with hydrochloric acid (CNC_{HCl}). Spin-coated films with two different configurations were prepared; the first with alternate layers of poly(allylamine hydrochloride) (PAHCl) and CNC, and the second with a single layer of PAHCl coated with multilayers of CNC. Film characteristics such as roughness, thickness, contact angle, orientation, gas permeability and gas selectivity were studied. Optical microscopy showed more homogeneous films of CNC_S compared to CNC_{HCl}. The surface charge of the crystals impacted the films' hydrophobicity, being highest for 25 alternate layers of PAHCl and CNC_{HCl}. The gas permeability coefficient was different for each film, depending primarily on the surface charge of the crystals and secondly on the film configuration. The films made with CNC_{HCl} displayed gas barriers with nitrogen and oxygen, and gas selectivity with some gas combinations. CNC_S films did not show gas selectivity. These results indicate that CNC with low surface charge can be further developed for gas separation and barrier applications.

1. Introduction

Polymer nanocomposites research has continued to advance since polymer nanocomposites were first prepared in 1990 (Kanatzidis, 1990). Polymer nanocomposites have been shown to have potential application in various sectors such as reinforced materials (Favier, Chanzy, & Cavaille, 1995; Petersson & Oksman, 2006) and gas barrier selectors (Belbekhouche, Bras, Siqueira, Chappey, & Lebrun, 2011), among others. However, due to the increase in the residual problems associated with the use of petroleum-based polymers, the focus in the improvement of polymer nanocomposites is on the use of renewable and natural constituents, like cellulose. Cellulose is a structural polysaccharide found in the cell wall of green plants and some algae (Rånby, Banderet, & Sillén, 1949). This polysaccharide is composed of an amorphous part and a crystalline part known as cellulose nanocrystals (CNC) or nanowhiskers (CNW) (for its rod-like shape). The dimensions of these crystals vary depending on the source from which they are isolated and, in general, CNCs fromwood source have a diameter of around 5 nm and a length of around 200 nm (Belbekhouche et al., 2011; Bondeson, Mathew, & Oksman, 2006; Herrera, Mathew, & Oksman, 2012a). This crystalline cellulose is isolated using acid hydrolysis, which cuts the native cellulose chain, consuming the amorphous part and leaving behind the crystalline part (Rånby et al., 1949). Due to the natural abundance of cellulose, bioinert behavior, low weight, and high strength and stiffness, these nanocrystals have served as an additive in the manufacture of composite materials in recent years (Chen, Liu, Chang, Cao, & Anderson, 2009; Cranston & Gray, 2008; Favier et al., 1995; Gindl & Keckes, 2005). Self-assembly of cellulose nanocrystals has been researched during the last years to obtain films with a high degree of crystal orientation to study the physical properties and crystalline structure of the cellulose (Belbekhouche et al., 2011; Cranston & Gray, 2008; Yoshiharu, Shigenori, Masahisa, & Takeshi, 1997). For a number of studies, the main interest has been the interaction between the crystals on the surface of the cellulosic material and the environment (Belbekhouche et al., 2011; Mohan, Kargl, Doliska, Vesel, & Koestler, 2011; Yoshiharu et al., 1997). For this reason, it is necessary to have a well-defined film with thickness in the nanometric range. Several studies have reported water contact angle and gas permeability properties of cellulose or associated nanocomposites (Belbekhouche et al., 2011; Favier et al., 1995; Kontturi, Johansson, Kontturi, Ahonen, & Thune, 2007; Mohan et al., 2011; Petersson & Oksman, 2006).

* Corresponding author. Tel.: +46 920 493371.
E-mail addresses: martha.herrera@ltu.se (M.A. Herrera), aji.mathew@ltu.se (A.P. Mathew), kristiina.oksman@ltu.se (K. Oksman).

http://dx.doi.org/10.1016/j.carbpol.2014.06.036
0144-8617/

Petersson and Oksman (2006) compared the barrier properties of polylactide acid (PLA) films reinforced with bentonite or microscrystalline cellulose (MCC) produced by solution casting. It was found that the oxygen permeability was not improved with the addition of MCC, as it was with the addition of the bentonite, which was attributed to lower dispersion of the MCC (Petersson & Oksman, 2006). Belbekhouche et al. (2011) found that solution-casted CNC films were more permeable to gases than films made of microfibrillated cellulose (MFC). This difference was attributed to a higher porosity in the CNC films and their different surface chemistry (Belbekhouche et al., 2011). The wettability of partly, and fully, regenerated cellulose model surfaces from spin-coated trimethylsilyl cellulose was investigated by Mohan et al. (2011). They reported that the wettability of polar and non-polar liquids increased with longer regeneration times. Therefore, it was assumed that the volatile distillation products tend to absorb partly on the regenerated films, which strongly influenced the film's wettability (Mohan et al., 2011). Isotropic films made entirely of CNC using solution casting were shown to perform well in blocking UV light, which makes them suitable in the food packaging industry, where UV protection is required. With the use of solution casting, the resulting films had a thickness of approximately 30 μm (Herrera et al., 2012a).

Spin coating has been shown to be a suitable method of preparing reproducible thin films of cellulose from a solution by removing the solvent with high-speed spinning (Kontturi et al., 2007). The spin coater technique has been used before for the preparation of open, sub-monolayer cellulose films, providing a novel approach for the interpretation of molecular architecture (Kontturi, Thune, Alexeev, & Niemantsverdriet, 2005). Different substrates in the production of CNC thin films have been used to investigate the effect of the substrate on the nanocrystal sub-monolayer (Kontturi et al., 2007). It has been shown that anionic CNC are absorbed on cationic substrates, while anionic CNC cause aggregation on anionic surfaces due to the repulsive forces (Kontturi et al., 2007). Self-assembled multilayered film of cellulose nanocrystals (aionic) and poly(allylamine hydrochloride) (PAHCl) (cationic) have been prepared with the spin coating technique (Cranston & Gray, 2008). Oriented nanocrystals and birefringence that varied with the relative location to the spin axis were found. With this layer-by-layer preparation method, smooth thin films on nanometric scale can be achieved (Aulin, Ahola, Josefsson, Nishino, & Hirose, 2009). These thin films are suitable for many different studies including X-ray diffraction, swelling, contact angle and barrier measurements.

The present work has been done with the objective of comparing two different configurations of spin-coated thin films prepared with CNC extracted from the same raw material source but using different acid hydrolysis methods. The analysis of the physical properties of the films can give insight into the types of applications for which they are best suited. For this reason, CNC surface charge, film appearance, roughness, thickness, orientation, water contact angle, and gas permeability and selectivity were studied.

2. Experimental procedure

2.1. Materials

An industrial residue from dissolving cellulose production (sulfite pulping) was kindly supplied by Domsjö Fabrikerna AB (Örnsköldsvik, Sweden). The residue is filtered from waste water and has a high cellulose content (approx. 96%). The material was received as non-dried cellulose pulp, filtered and with a moisture content of 42%. The residue was used, as received, for extraction of cellulose nanocrystals by acid hydrolysis.

Commercial poly(allylamine hydrochloride) (PAHCl) with a molecular weight of 15,000 g/mol was obtained from Sigma-Aldrich. The PAHCl was used as anchoring layer for CNC in the production of the spin-coated films.

2.2. Acid hydrolysis

Colloidal suspensions of CNC were prepared with sulfuric acid (CNC_S) and hydrochloric acid (CNC_{HCl}). In sulfuric acid (H_2SO_4) hydrolysis, 60 g of cellulose residue was placed in a suspension of 65% H_2SO_4 at 40 °C under mechanical stirring for 30 min, using the procedure developed by Bondeson et al. (2006). The final suspension was concentrated to a concentration of 0.83 wt% cellulose nanocrystals. In hydrochloric acid (HCl) hydrolysis, 50 g of the cellulose residue was placed in a solution of 14.4% of HCl at 80 °C for 225 min, according to a previously reported procedure (Bondeson et al., 2006). The turbid solution was concentrated to a concentration of 0.79 wt% of cellulose nanocrystals. The CNC obtained from both hydrolysis procedures were in form of a colloidal suspension of 1 wt% concentration and the crystals diameters were between 3 and 7 nm, as measured from the height using AFM. The length of the crystals was estimated in our previous study to be between 300 and 500 nm but due to limitations of AFM this is only an approximation (Herrera, Mathew, & Oksman, 2012b).

2.3. Conductometric titration

The surface charge of the crystals was measured using a Metler Toledo SevenEasy™ conductometer and an InLab® 73X sensor (Schwerzenbach, Switzerland). Titration was done to measure the amount of negative charge on the CNC surfaces following a standard route for strong acid versus strong base (Abitbol, Kloser, & Gray, 2013; Araki, Wada, Kuga, & Okana, 1999; Herrera et al., 2012a, 2012b). This method is based on change in conductivity when the charged groups on the CNC surface have been neutralized with NaOH.

2.4. Substrates

2.4.1. Glass

Borosilicate cover glass of $18 \times 18\,mm^2$ and thickness No. 1 (0.16 mm) from VWR International was used. The glass substrates were cleaned with a piranha solution (3:1 concentrated sulfuric acid to hydrogen peroxide) for 30 min and rinsed with fresh deionized water and spin-coated directly.

2.4.2. Filter paper

Whatman ME25 membrane filter (mixed cellulose ester), with a pore size of 0.45 μm, was cut into circles of 25 mm in diameter. The substrates were rinsed three times with the constant addition of acetone and deionized water prior the spin coating.

2.5. Thin film preparation

A Brewer Science Inc. 200X spin coater (Rolla, USA) was used for the deposition of the thin films over the two different substrates. For each substrate two different thin film configurations were made.

In the first configuration alternate layers of PAHCl and CNC were prepared. This procedure is a slightly modified means of polyelectrolyte multilayer film construction used by Cranston & Gray, (2008) and Aulin et al. (2009). Five hundred microliter of a 0.6% PAHCl solution (positively charged polyelectrolyte) was placed on the substrate, accelerated at 1260 rpm/s and spun at 3000 rpm for 40 s. Then, the surface was washed three times using 1000 μL of deionized water with the same spinning conditions. Thereafter, 500 μL of CNC suspension was added onto the washed layer and

spin coated using the same conditions and followed by three washing steps. One alternate layer is designed as one thin layer of PAHCl and a layer of CNC. Alternate layered films were created with both kinds of cellulose nanocrystals (CNC_S and CNC_{HCl}) containing totally 50 layers (25 layers of PAHCl intercalated with 25 layers of CNC). These films are named 25 CNC_S and 25 CNC_{HCl}.

In the second configuration one single layer of PAHCl coated with multilayers of CNC was prepared following the same spinning conditions as in the first configuration. The multilayer consists of 25 layers of CNC. These samples are named 1 + 25 CNC_S and 1 + 25 CNC_{HCl}. The films were dried and kept under ambient conditions before the characterization. The deposition of CNC films on the filter paper was done following the same conditions as explained above.

2.6. Optical microscope

The films were examined under a polarized optical microscope ECLIPSE MA200 Nikon (Tokyo, Japan). The thin films, on the glass substrate, were analyzed on a bright field to evaluate the homogeneity. The images were studied using the NIS-Elements BR 4.00.008 software, included with the microscope.

2.7. Atomic force microscopy

Topographical features of the thin films were characterized by atomic force microscopy (AFM) in tapping mode with a Nanoscope V microscope Veeco Instruments (Santa Barbara, CA, USA). A noncentral piece from the glass substrate with the thin film was cut and placed over a standard AFM sample holder. Height and amplitude images were recorded using a resonance frequency of 304 kHz. The roughness (*Rq*) and the thickness values were measured from the height images, and the orientation from the amplitude images. The roughness values reported are the average of at least five different measurements on the surface area of 50 μm^2 and the thicknesses of the films were obtained by digital analysis of the scratch-height in at least four different positions on at least four different images of 50 μm^2. All the measurements were done in air at room temperature.

2.8. Contact angle

For the static contact angle measurements a dynamic absorption and contact angle tester "fibro dat 1120" FIBROSystem AB (New Castle, USA) was used. One drop of water (4 μL) is placed onto the coated glass surface. The software of the instrument calculates the contact angle at three different times of the drop life (0.1 s, 1 s, and 10 s), but for the calculations, only the contact angle at 1 s was taken into account.

2.9. Gas permeability

Hydrogen (H_2), nitrogen (N_2), helium (He), carbon dioxide (CO_2) and oxygen (O_2) permeability were measured, separately, for the CNC films spin coated onto filter substrate. H_2 and He are gases that are not commonly used to measure the gas permeability of films. However, in this study those gases were tested to see the interaction of gases with similar molecular size but different reactivity with the films. A constant gas flow with a pressure of 0.2 bar (15 cmHg) was applied to the films. The exit flow was registered with an Agilent Technologies ADM2000 universal gas flow meter 2850 (Wilmington, USA). The basic factors that characterize a film separation execution are the permeability coefficient *P* and the ideal selectivity $\alpha_{A/B}$ (Belbekhouche et al., 2011; Van Krevelen & Nijenhuis, 2009).

The permeability coefficient *P* is calculated using the variable pressure model (Belbekhouche et al., 2011; Joly, Le Cerf, Chappey, Langevin, & Muller, 1999; Van Krevelen & Nijenhuis, 2009). It was assumed that the incoming gas pressure p_1 is significantly higher than the exit gas pressure p_2 (Belbekhouche et al., 2011; Joly et al., 1999). The model describes *P* of a gas molecule A as the product of the steady-state gas exit flow in a specific exposed area of the film J_{st}, and the film thickness *d*, divided by the inlet gas pressure p_1 (Joly et al., 1999; Park & Lee, 2008; Van Krevelen & Nijenhuis, 2009).

$$P = \frac{J_{st} \times d}{p_1} \quad (1)$$

The unit in which *P* is described is known as Barrer, in honor of Professor R.M. Barrer, who was a pioneer of permeability studies (Stern, 1968). As J_{st} is expressed in cm^3 of the gas at standard temperature, a pressure (STP)/s cm^2, *d* is expressed as cm and p_1 in cmHg; the unit of *P*, the Barrer, is expressed as 10^{-10} cm^3 (STP) cm/s cm^2 cmHg (Stern, 1968).

The ideal selectivity ($\alpha_{A/B}$) is described as the ratio of the permeability coefficients for two different gases *A* and *B* (Van Krevelen & Nijenhuis, 2009):

$$\alpha_{A/B} = \frac{P_A}{P_B} \quad (2)$$

where P_A is the more permeable gas and P_B the less permeable gas. For each film, permeation experiments were carried out four times for each gas. Three films from each configuration were tested.

3. Results and discussion

3.1. Nanocrystal characteristics

The surface charge of nanocrystals provides important information about the surface characteristics of the thin films prepared from them. Negative and positive surfaces are more hydrophilic than the neutral surface (Marchessault, 1959; Sanchez, 2003). The surface charge is also important because negatively charged CNCs produce colloidal suspensions with better stability than crystals with no surface charge (Favier et al., 1995; Park & Lee, 2008). Neutral CNC cannot form a colloidal suspension because of flocculation (Roman & Winter, 2004). This can be a problem for film homogeneity, where aggregated CNCs may be found in films produced with low surface charged crystals. The different surface charges depend on the acids used isolating the CNC. It is well known that the use of sulfuric acid will result in the sulfate groups on crystal surfaces (Oksman, Etang, Mathew, & Jonoobi, 2011; Roman & Winter, 2004) while the use of hydrochloric acid leaves CNC with very low charge (Araki et al., 1999).

The surface charge of the H_2SO_4 crystals (CNC_S) was measured to 339 ± 9 μmol/g, while the surface charge of HCl crystals (CNC_{HCl}) was too low to be measured. This low surface charge was expected and earlier reported by Araki et al. (1999), who reported that the surface charge of the cellulose nanocrystals, extracted by hydrochloric acid hydrolysis, was 2 μmol/g (Araki et al., 1999).

3.2. Thin film characteristics

Optical microscope images of the spin-coated films with the different configurations on the glass substrate are seen in Fig. 1. The optical microscope observation was done to verify the complete coverage and homogeneity of the films on the glass substrate. It may be noted that the CNC_S films with both configurations were more homogeneous than the CNC_{HCl} films, where some darker areas indicate a higher crystal concentration (or density).

Scanning electron microscopy was also done to obtain more detailed information about the microstructure of the films. Fig. 2

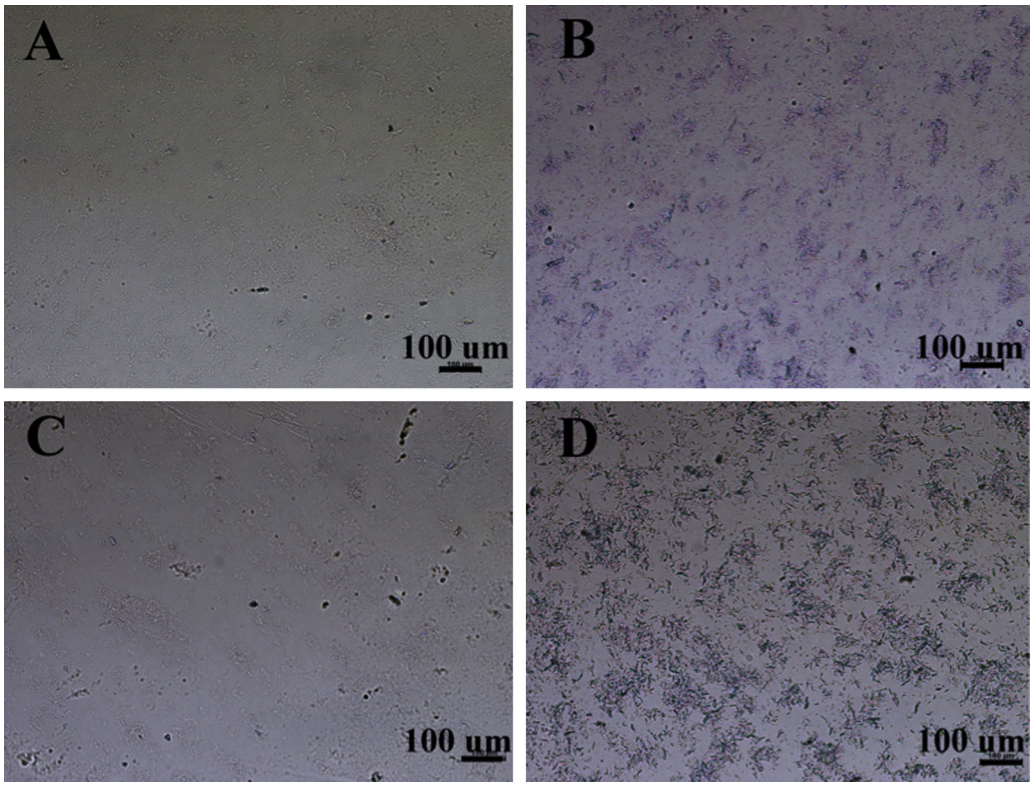

Fig. 1. Polarized optical microscope images of the films deposited on a glass substrate of (A) 25 CNC_S, (B) 25 CNC_{HCl}, (C) 1 + 25 CNC_S, and (D) 1 + 25CNC_{HCl}.

shows microstructures of the films spin-coated on the filter substrate. In Fig. 2A the naked substrate can be seen. Fig. 2B and D shows that the films of CNC_S are more homogeneous and that the filter surface is covered by small whisker-like particles.

The films with CNC_{HCl} (Fig. 2C and E) show that the filter surface is covered by aggregated crystals and these film surfaces are also clearly rougher. The agglomeration observed on the films made with CNC_{HCl} is expected because of the lack of the surface charge. Another possible explanation for the agglomerates observed in these surfaces is the accumulation of the crystals during the layer-by-layer deposition. These SEM images support the optical microscopy study on the glass substrate, shown in Fig. 1.

The roughness values were obtained using AFM topography images, and are shown as mean values (*Rq*) for each type of crystal and film configuration in Table 1. It can be seen that the film configuration and surface characteristics of the crystals affected the roughness of the films. The films with CNC_{HCl} were rougher when compared with the films of CNC_S. The films with 25 CNCs had approximately three times higher roughness than the film with 1 + 25 CNC_S, which showed the lowest roughness values (52 nm). These values are higher than earlier reported for spin-coated thin CNC films by Cranston and Gray (2008), who reported a roughness of 4 nm and by Aulin et al. (2009), who reported a roughness of 5 nm. The reason for higher roughness in our study might be that some larger particles or agglomerates are present, especially in the case of CNC_{HCl}.

From Table 1, it can also be seen that the roughness for 1 + 25 CNC_{HCl} films is higher than its thickness. This result suggests a high concentration of defects along the film. This higher concentration of defects, which are the agglomerations observed on the SEM images, may be caused by the lack of surface charge of the crystals extracted from HCl.

Fig. 3 shows the AFM topography images of the films with different configurations; a *z*-scale of 500 nm was used. It is clearly seen that the films with CNC_{HCl} are rougher than CNC_S films. Also, it is possible to see that the film configuration affects the roughness; the films with monolayers of CNC are generally smoother than those with the alternate layer structure. Amplitude images in Fig. 3 do not show any specific orientation.

3.3. Contact angle

The contact angle measurements were done to see if there was a relation between the contact angle value, roughness in surface and crystals with different surface charge. Table 1 presents the contact angle values obtained for the different thin films produced on the glass substrates. It is known that the PAHCl has a positive charge, and the CNC_S films are negatively charged, as reported in Section 3.1. When these two materials are connected in an alternately layered configuration (25 CNC_S), it is believed that the charges are neutralized, leaving a neutral surface. Something similar may happen with the 1 + 25 CNC_{HCl} film. Due to the very low

Table 1
Surface roughness, contact angle, and thickness of the spin-coated thin films on glass substrate. The numbers in the table are the average and standard deviations of the measured values of each property.

	Glass	25 CNC_S	25 CNC_{HCl}	1 + 25 CNC_S	1 + 25 CNC_{HCl}
Roughness (nm)	5	150 ± 53	299 ± 46	52 ± 10	338 ± 129
Contact angle (°)	57.8 ± 2.7	46.5 ± 4.0	58.9 ± 2.3	39.7 ± 6.1	46.2 ± 8.9
Film thickness (nm)	–	356 ± 76	425 ± 80	265 ± 23	277 ± 40

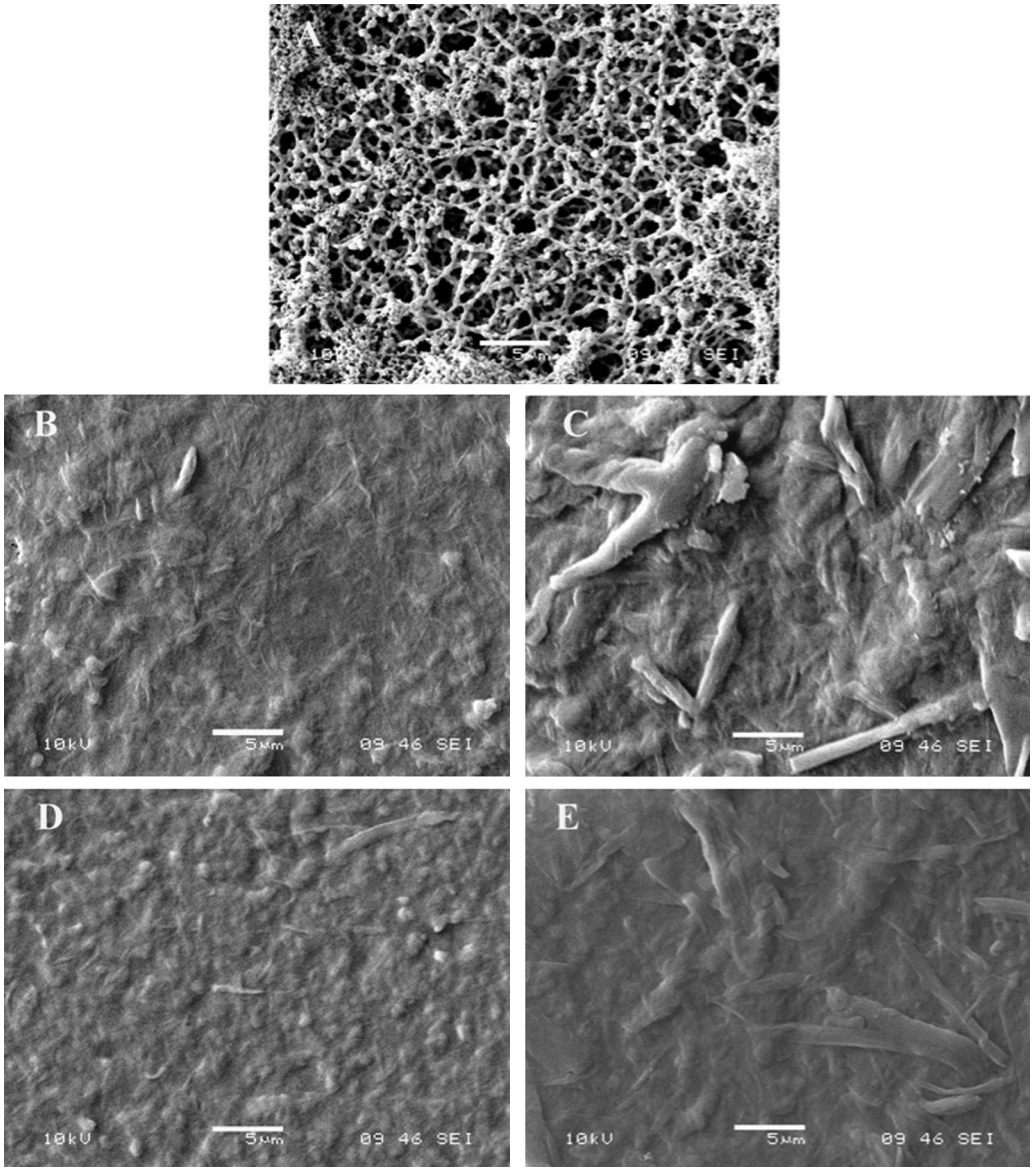

Fig. 2. SEM images of the CNC films deposited on the filter substrate. (A) Naked filter, (B) 25 CNC_S, (C) 25 CNC_{HCl}, (D) 1 + 25 CNC_S, and (E) 1 + 25CNC_{HCl}.

surface charge of the crystals it can be assumed that the film surface will be neutral. In the case of 1 + 25 CNC_S films, it is believed that the single layer of PAHCl is not enough to neutralize the surface charge effect of the crystals, leading to a negatively charged surface. The film with 25 CNC_{HCl}, is positive due to the contribution of the PAHCl. These assumptions are confirmed with the measured contact angles. The bipolar nature of water molecules is the reason that the film with 1 + 25 CNC_S has the lowest and the film with 25 CNC_{HCl} has the highest contact angle. The molecular re-orientation of the water molecule on charged surfaces has been previously studied and it was found that when surfaces were positively charged, the oxygen (negative part on the molecule of water) would face the surface. However, if the surfaces are negative, the oxygen will point away from the surface (Sanchez, 2003).

A schematic representation of this behavior is shown in Fig. 4. As seen, when the substrate is negatively charged and the oxygen is facing toward the substrate, the contact angle is higher than when the substrate is negative and the oxygen faces away from it. This behavior is seen also in the values obtained on the films with different surface charges.

It is also known that the contact angle is greatly affected by the chemical composition and topographical structure of the surface. A hierarchical roughness (combination of micro and submicrometer-sized roughness) and a highly hydrophobic surface can be used for the manufacture of materials with super-hydrophobicity and low adhesion (Bhushan, Jung, & Koch, 2009; Phani, Grossi, Passacantando, & Santucci, 2007). Phani et al. (2007) prepared thin films using carbon nanotubes and were able to increase the film roughness from 8 ± 1 nm to 32 ± 1 nm by annealing. With this small increase in roughness, they changed the hydrophobic film surface (contact angle higher than 90°), to super-hydrophobic (contact angle higher than 150°) (Bhushan et al., 2009; Phani et al., 2007). Comparing this to the present study it can be concluded that an increase in the film roughness can lead to an increase in the contact angle. In our case the increase in roughness did not lead to such dramatic change of the hydrophobicity.

3.4. Thickness

The film thickness value is an important parameter for the calculation of the gas permeability; for this reason the

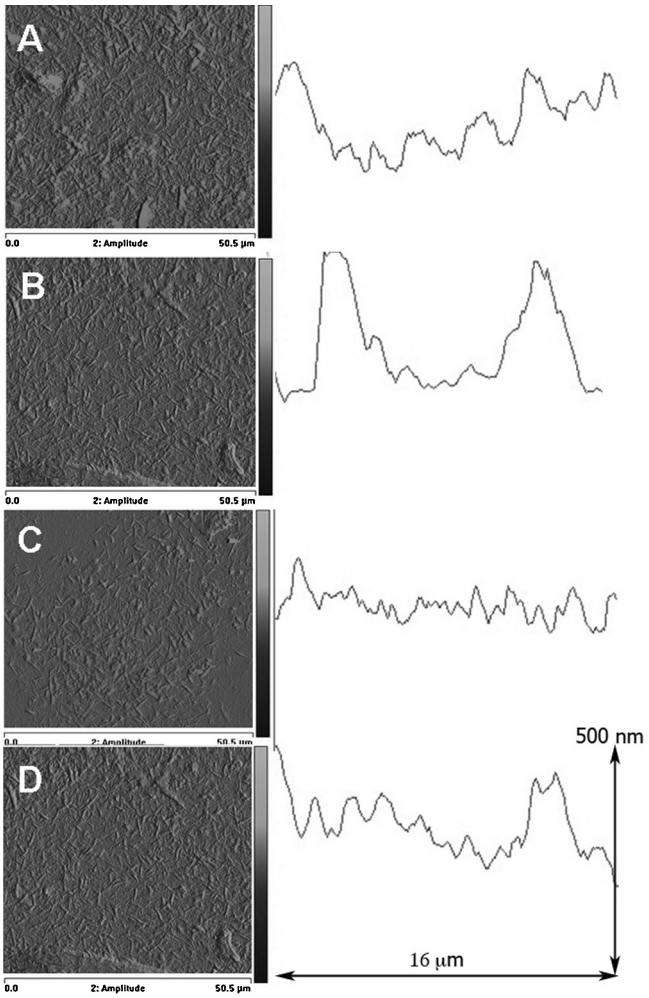

Fig. 3. $50 \times 50\ \mu m^2$ amplitude images obtained from the AFM analysis of the spin-coated thin films on the glass substrate (A) 25 CNC_S, (B) 25 CNC_{HCl}, (C) 1 + 25 CNC_S, and (D) 1 + 25 CNC_{HCl}.

thickness was measured with scratch-height analyses (Cranston & Gray, 2008). When the scratch-height analysis by AFM was compared with other film thickness analysis methods like ellipsometry, wavelength-dependent and angle-dependent optical reflectometry, this technique proved to be a reliable method for measuring the thickness of thin films (Cranston & Gray, 2008). This test was done on the films prepared on the glass substrate because the filter paper did not allow the utilization of scratch-height analyses. However, it is believed that the thicknesses of the films on both the substrates are similar (but not the roughness). The thickness of the spin-coated films ranged from 265 nm for 1 + 25 CNC_S to 425 nm for 25 CNC_{HCl}, as shown in Table 1. The measured thicknesses are similar to earlier reported values (Cranston & Gray, 2008). As expected, the samples with monolayered structure were thinner.

3.5. Gas permeability

To tailor good barrier properties for the thin films it is important to understand the size effect of the gas molecules, their interaction with the barrier layer and the morphology of the barrier layer. It is known that gas transport through films can occur by five idealized mechanisms: (1) molecular sieving, where the gases are separated by their sizes, (2) surface diffusion, where gas molecules with higher polarity are selectively adsorbed and diffused through the film, (3) capillary condensation, where the gas condenses in the pores of the film, diffuses as a liquid through the material and exits as a gas again, (4) Knudsen diffusion, where the gases are separated based on the difference in the mean path of the gas molecule through the film and (5) selective adsorption diffusion, where the gases are separated by their solubility within the film and their diffusion through it (Park & Lee, 2008).

The typical permeability coefficient (P) for polymer films decreases with the increase in the molecular diameter of the gas molecules (Gindl & Keckes, 2005). The molecule diameters of the gases used are: N_2 = 0.36 nm, O_2 = 0.35 nm, CO_2 = 0.33 nm, H_2 = 0.29 nm, and He = 0.26 nm (Belbekhouche et al., 2011; Park & Lee, 2008) and according to this theory, the permeability values should follow the order: $P_{N_2} < P_{O_2} \approx P_{CO_2} < P_{H_2} < P_H$ (Joly et al., 1999; Roman & Winter, 2004). However, the permeability coefficient data presented in Table 2 show that this pattern was not followed by any of the studied films and it is possible that the size differences in the studied gases are not significant enough to impact the permeability.

The results in this study contradict a previous study by Belbekhouche et al. (2011), where it was shown that the gas permeability depended on the predicted kinetic radius for the films made of CNC_S. But the permeability coefficients presented were a magnitude higher than measured in the current study, in spite of higher film thickness. The authors also assumed that both the chemical composition and structure of the films could affect the gas permeability (Belbekhouche et al., 2011).

Moreover, the characteristics of the nanocrystals affected the gas permeability coefficient, as seen in Table 2. When the same film configurations with different CNC are compared, it can be seen that the gas permeability for the films of CNC_S is higher, except for hydrogen (H_2) and helium (He). In this specific case, it is possible that the inert nature of helium plays an important role. The lack of interaction between the inert gas (He) and the film leads to a lower solubility, adsorption and diffusion of the gas through the material. Also, another factor that could affect the gas permeability is the molecular weight of these two gases. According to Graham's law of diffusion, the diffusion rate of the gases is inversely proportional to the square root of their molecular weight (Zumdahl, 2009, chap. 5). Following Graham's law and knowing the molecular weights of He and H_2 (4 and 2 g/mol, respectively), it can be predicted that the diffusion of He would be 0.7 times the diffusion of H_2. As the permeability is directly proportional to the diffusion (Park & Lee, 2008) it can be considered that $P_{He} \approx 0.7 P_{H_2}$. Fig. 5 shows that the experimental values of P from Table 2 fit well with the predicted

Fig. 4. Schematic representation of the contact angle of negatively and positively surfaces.

Table 2
Permeability coefficient P of H_2, N_2, He, CO_2 and O_2 for the different CNC film configurations measured at standard temperature and pressure. The numbers in the table are the average and standard deviations of the measured values.

		25 CNC_S	25 CNC_{HCl}	1 + 25 CNC_S	1 + 25 CNC_{HCl}
P (10^3 Barrer)	H_2	24.0 ± 2.2	51.5 ± 1.2	12.7 ± 0.6	43.3 ± 2.9
	N_2	12.3 ± 0.1	3.8 ± 1.1	10.5 ± 0.1	1.6 ± 0.4
	He	14.8 ± 1.0	35.5 ± 7.8	7.8 ± 0.4	22.0 ± 0.3
	CO_2	31.5 ± 0.1	29.2 ± 0.1	24.9 ± 0.0	17.0 ± 0.8
	O_2	11.3 ± 0.1	2.6 ± 0.6	10.3 ± 0.1	2.5 ± 0.5

Barrer = 10^{-10} cm^3 (STP) cm/cm^2 s cmHg.

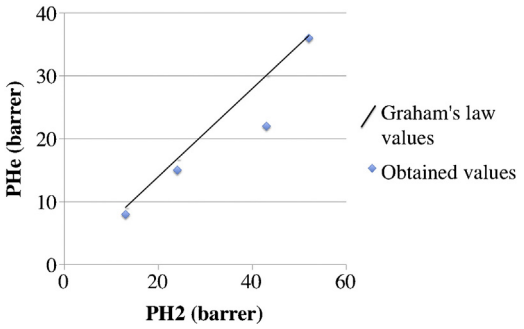

Fig. 5. Graham's law model values for He depending on H_2 compared with the obtained experimental values.

Table 3
Selectivity values ($\alpha_{A/B}$) for the different films and gases tested.

$\alpha_{A/B}$	25 CNC_{HCl}	1 + 25 CNC_{HCl}
H_2/N_2	13.5	26.9
H_2/O_2	20.1	17.7
H_2/He	–	13.7
N_2/CO_2	–	10.6
He/O_2	13.9	–
CO_2/O_2	11.4	–

values of Graham's law. This suggests that in the case of He and H_2 the weight difference and not the kinetic radius difference was the main issue.

When different film configurations made of the same type of crystals are compared, it is important to point out that the gas diffusion occurs mainly through the non-crystalline part of the films. Subsequently, the more crystalline a film is, the lower the gas permeability coefficient. This occurs because the crystalline regions tend to obstruct the diffusion of the gas molecule and increase the average length of the path they have to travel through the film (Van Krevelen & Nijenhuis, 2009). This phenomenon is known as tortuosity. From Table 2 it can be observed that the 25 CNC films showed higher P than 1 + 25 CNC films. This shows that the gas molecules can diffuse easier through the film with higher polymer content (lower tortuosity). A schematic representation of this behavior can be seen in Fig. 6.

It is worth noting that the food packaging industry is especially interested in the gas barrier properties against oxygen and nitrogen. Nitrogen is used as an efficient, cost-effective way to displace oxygen and moisture to avoid product deterioration and thereby better preserve the food for a longer time. The values for oxygen and nitrogen permeability for materials made with CNC_{HCL} obtained in this study are very promising when compared with reported values for oxygen and nitrogen permeability of packaging materials such as poly(ethylene), poly(vinyl alcohol), and cellulose (cellophane) (Singh & Heldman, 2009). For this reason it is important to point out that the films made with CNC_{HCl}, presented the lowest gas permeability values for oxygen and nitrogen, making these films especially suitable as a gas barrier in food packaging applications.

The selectivity value ($\alpha_{A/B}$) for two different gases, A and B, is the ratio of the permeability coefficient and it is affected by the differences in the solubility and/or diffusivity of the gases in the films (Park & Lee, 2008). When this value is higher than 10, the film presents gas selectivity behavior (Belbekhouche et al., 2011). The data in Table 3 were calculated using Eq. (2) and only the values higher than 10 are reported.

The films with CNC_S did not present any gas selectivity; similar results were reported by Belbekhouche et al. (2011), where no gas selectivity for CO_2, O_2, and N_2 was observed. CNC_{HCl} films showed gas selectivity for some gas combinations in this study and were highest for H_2/N_2 and H_2/O_2. It could be proved that it was not only the type of the crystals which affected the selectivity, but also the configuration of the films. These results confirm that the films made with the neutral nanocrystals (lower surface charge) presented gas selectivity in some gas combinations, and the films made of the CNC_S (higher surface charge) did not show that behavior.

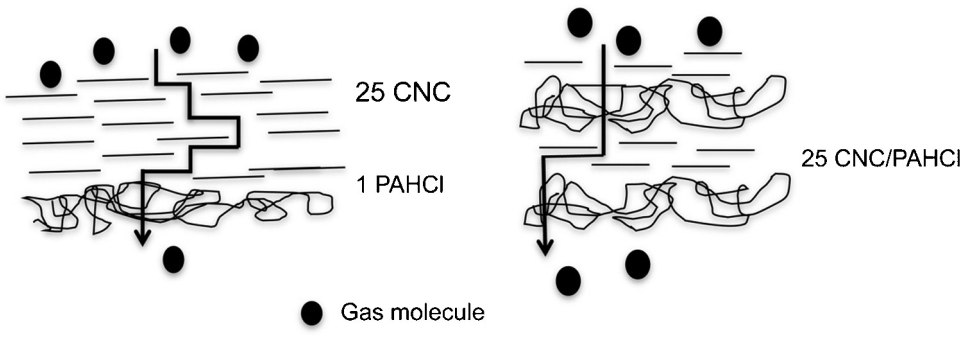

Fig. 6. Schematic of the gas molecule diffusion in the film configurations used.

4. Conclusions

Cellulose nanocrystals were extracted from an industrial residue from special cellulose production by acid hydrolysis with either sulfuric or hydrochloric acid. The difference in the acid hydrolyses resulted in different surface charged crystals.

Thin spin-coated films with two different configurations on two different support layers were prepared; the first with alternate layers of poly(allylamine hydrochloride) (PAHCl) and CNC, and the second with a single layer of PAHCl coated with multilayers of CNC. The film thickness varied from 425 nm for the 25 CNC_{HCl} films to 265 nm for the 1 + 25 CNC_S films.

The hydrochloric acid crystals (CNC_{HCl}) resulted in films with lower homogeneity, higher roughness, low permeability for N_2 and O_2 and also gas selectivity for some gas combinations. The sulfuric acid crystals (CNC_S) resulted in smooth and homogeneous films but higher permeability in general and no selectivity.

It can be concluded that the surface charge of the crystals affects their processing ability. It is easier to make thin films with CNC_S because of their colloidal suspension stability and the electrostatic interaction with the positively charged polymer phase.

Further studies using CNC_{HCl} to prepare films with improved homogeneity with better dispersion and distribution of crystals will be the next step to improve their gas selectivity and gas barrier properties in different environments.

Acknowledgements

We would like to thank Bio4Energy (Sweden) for financial support for this study. Domsjö Fabrikerna AB, Örnsköldsvik, Sweden is gratefully acknowledged for supplying the cellulose residue from their special cellulose production. We would like to thank doctoral student Erik Sjöberg at Division of Chemical Engineering at LTU for his help with the gas permeability measurements.

References

Abitbol, T., Kloser, E., & Gray, D. G. (2013). Estimation of the surface sulfur content of cellulose nanocrystals prepared by sulfuric acid hydrolysis. *Cellulose*, *20*, 785–794.

Araki, J., Wada, M., Kuga, S., & Okana, T. (1999). Influence of surface charge on viscosity behavior of cellulose microcrystal suspension. *Journal of Wood Science*, *45*, 258–261.

Aulin, C., Ahola, S., Josefsson, P., Nishino, T., & Hirose, Y. (2009). Nanoscale cellulose films with different crystallinities and mesostructures—Their surface properties and interaction with water. *Langmuir*, *25*, 7675–7685.

Belbekhouche, S., Bras, J., Siqueira, G., Chappey, C., & Lebrun, L. (2011). Water sorption behavior and gas barrier properties of cellulose whiskers and microfibrils films. *Carbohydrate Polymers*, *83*, 1740–1748.

Bhushan, B., Jung, Y., & Koch, K. (2009). Micro-, nano- and hierarchical structures for superhydrophobicity, self-cleanning and low adhesion. *Philosophical Transactions of The Royal Society A Mathematical Physical and Engineering Sciences*, *367*, 1631–1672.

Bondeson, D., Mathew, A., & Oksman, K. (2006). Optimization of the isolation of nanocrystals from microcrystalline cellulose by acid hydrolysis. *Cellulose*, *13*, 171–180.

Chen, Y., Liu, C., Chang, P., Cao, X., & Anderson, D. (2009). Bionanocomposites based on pea starch and cellulose nanocrystals hydrolyzed from pea hull fibre: Effect of hydrolysis time. *Carbohydrate Polymers*, *76*, 607–615.

Cranston, E. D., & Gray, D. G. (2008). Birefringence in spin-coated films containing cellulose nanocrystals. *Colloids and Surfaces A: Physicochemical and Engineering Aspects*, *325*, 44–51.

Favier, V., Chanzy, H., & Cavaille, J. (1995). Polymer nanocomposites reinforced by cellulose whiskers. *Macromolecules*, *28*, 6365–6367.

Gindl, W., & Keckes, J. (2005). All-cellulose nanocomposite. *Polymer*, *46*, 10221–10225.

Herrera, M. A., Mathew, A. P., & Oksman, K. (2012a). Comparison of cellulose nanocrystals extracted from industrial bio-residue and commercial microcrystalline cellulose. *Materials Letters*, *71*, 28–31.

Herrera, M. A., Mathew, A. P., & Oksman, K. (2012b). Characterization of cellulose nanowhiskers: A comparison of two industrial bio-residues. *IOP Conference Series: Materials Science and Engineering*, *31*, 012006.

Joly, C., Le Cerf, D., Chappey, C., Langevin, D., & Muller, G. (1999). Residual solvent effect on the permeation properties of fluorinated polyimide films. *Separation and Purification Technology*, *16*, 47–54.

Kanatzidis, M. G. (1990). Conductive polymer/oxide bronze nanocomposites. Intercalated polythiophene in V_2O_5 xerogels. *Chemistry of Materials*, *2*, 222–224.

Kontturi, E., Johansson, L., Kontturi, K., Ahonen, P., & Thune, P. (2007). Cellulose nanocrystal submonolayers by spin coating. *Langmuir*, *23*, 9674–9680.

Kontturi, E., Thune, P., Alexeev, A., & Niemantsverdriet, J. (2005). Introducing open films of nanosized cellulose—Atomic force microscopy and quantification of morphology. *Polymer*, *46*, 3307–3317.

Marchessault, R. H. (1959). Liquid crystal systems from fibrillar polysaccharides. *Nature*, *184*, 632–633.

Mohan, T., Kargl, R., Doliska, A., Vesel, A., & Koestler, S. (2011). Wettability and surface composition of partly and fully regenerated cellulose thin films from trimethylsilyl cellulose. *Journal of Colloid and Interface Science*, *358*, 604–610.

Oksman, K., Etang, J. A., Mathew, A. P., & Jonoobi, M. (2011). Cellulose nanocrystals separated from a bio-residue from wood bioethanol production. *Biomass and Bioenergy*, *35*, 146–152.

Park, H. B., & Lee, Y. M. (2008). Polymeric membrane materials and potential use in gas separation. In *Advanced membrane technology and applications*. New Jersey: John Wiley & Sons.

Petersson, L., & Oksman, K. (2006). Biopolymer based nanocomposites: Comparing layered silicates and microcrystalline cellulose as nanoreinforcement. *Composites Science and Technology*, *66*, 2187–2196.

Phani, A. R., Grossi, V., Passacantando, M., & Santucci, S. (2007). The role of nanoscale topography on super-hydrophobicity: A study of fluoro-based polymer film on vertical carbon nanotubes. *Journal of Experimental Nanoscience*, *2*, 63–71.

Roman, M., & Winter, W. (2004). Effect of sulfate groups from sulfuric acid hydrolysis on the thermal degradation behavior of bacterial cellulose. *Biomacromolecules*, *5*, 1671–1677.

Rånby, B., Banderet, A., & Sillén, L. (1949). Aqueous colloidal solutions of cellulose micelles. *Acta Chemica Scandinavica*, *3*, 649.

Sanchez, C. (2003). Molecular reorientation of water adsorbed on charged Ag(1 1 1) surfaces. *Surface Science*, *527*, 1–11.

Singh, R., & Heldman, D. (2009). Packaging concepts. In *Introduction to food engineering*. UK: Elsevier.

Stern, S. (1968). The barrer permeability unit. *Journal of Polymer Science, Part A-2: Polymer Physics*, *6*, 1933–1934.

Van Krevelen, D. W., & Nijenhuis, K. (2009). *Properties of polymers—Their correlation with chemical structure; their numerical estimation and prediction from additive group contributions* (4th ed.). Netherlands: Elsevier (Chapter 18).

Yoshiharu, N., Shigenori, K., Masahisa, W., & Takeshi, O. (1997). Cellulose microcrystal film of high uniaxial orientation. *Macromolecules*, *30*, 6395–6397.

Zumdahl, S. (2009). *Chemical principles* (6th ed.). Boston: Houghton Mifflin Company.